CrossMark

The Effect of Grain Size on Fatigue Crack Propagation in Commercial Pure Titanium Investigated by Acoustic Emission

Lifei Li, Zheng Zhang, and Gongtian Shen

The effect of grain size on fatigue crack propagation and the corresponding acoustic emission (AE) characteristics of commercial pure titanium (CP-Ti) were investigated at room temperature. After a four-point bending fatigue testing, the fatigue features and AE source mechanisms were discussed, combined with microstructural and fractographic observations. The results showed that the increased grain size had little effect on the stable propagation rate of fatigue crack; however, a significant increase in the AE counts rate was observed. During crack stable propagation, the relationship between the AE counts rate and the fatigue stress intensity factor range was generally in accordance with the Pairs law, with the exception of some local fluctuations due to regional twin paling. While lenticular twins appeared dispersively along the crack, twin palings were observed occasionally at the edge of the crack. Twin paling occurrence was more frequent in the specimens with larger grains than in those with smaller grains. This suggests that twin discontinuously played a role in the fatigue process in this CP-Ti, and that the AE technique is sensitive to crack propagation and twinning events during fatigue.

1. Introduction

Due to its remarkable corrosion resistance, good mechanical properties, and machinability, titanium and its alloys have been widely used in pressure vessels and pipelines for application in corrosive environments. Because of the application of cyclic loading on equipment components and the corresponding potential for fatigue damage, it is essential for safety to predict the integrity of these components. Changes in the microstructure can alter the fatigue behavior of metal material. A considerable amount of work has been concerned with the effect of grain size on the fatigue crack initiation and on the fatigue life of titanium alloys (Ref 1-5). However, only a few works have focused on the influence of grain size on fatigue crack propagation behavior. From analysis of five conditions of beta-annealed titanium alloys, Yoder et al. (Ref 6) found that the crack growth rate varied inversely with the mean Widmanstätten packet size. For α-titanium alloys under low stress level fatigue, Robinson and Beevers (Ref 7) observed that increasing grain size produced a reduction in fatigue crack propagation rate under low values of the stress intensity factor

range. For long crack growth in Ti-6Al-4V, Oberwinkler (Ref 8) observed that the crack propagation rate in the Paris regime was independent of the microstructure.

Acoustic emission (AE) is an elastic stress wave that is generated by a rapid release of energy from a localized source within a stressed material (Ref 9). Recently, the AE technique appears to be an effective nondestructive evaluation method for in-site monitoring to detect growing flaws (Ref 9-11). To further understand AE, some investigations associated the AE source mechanisms with microstructures and microdamage events. Kohn et al. (Ref 12) studied the influences of equiaxed and lamellar microstructures of Ti-6Al-4V on failure behavior by AE monitoring. They concluded that more interfaces and larger grain sizes in the lamellar microstructure accounted for the more cleavage and intergranular fractures and the greater amount of AE than the equiaxed microstructure. In a fracture toughness test of Ti-8Al-1Mo-1V alloy, Mashino et al. observed that the specimen with a acicular α microstructure had higher fracture toughness than the specimen with a equiaxed α one, and the number of AE events stemming from microcracks generation were larger in the acicular microstructure (Ref 13). By monitoring the crack initiation and propagation in Ti-6Al-4V, Kohn et al. reported that AE can detect the crack incipient extension even on the magnitude of 10 μm; furthermore, the variation of the AE event rate corresponded to the changes of crack extension rate, which indicated crack growth from steady propagation to rapid propagation (Ref 14). The stage of fatigue crack stable propagation occupies a considerable proportion of the fatigue life. For better application of AE for fatigue damage monitoring, the aim of the present work is to investigate the effect of grain size on the behavior of crack stable growth in titanium. The AE signals generated during fatigue test were compared and analyzed. Complemented with the microstructural and fractographic observations, the AE source mechanisms were illustrated based on the twins with different morphologies.

Lifei Li and **Zheng Zhang**, Key Laboratory of Aerospace Materials and Performance (Ministry of Education), 8th Lab of the School of Material Sciences and Engineering, Beihang University, No. 37 Xueyuan Road, Haidian District, Beijing 100191, China; and **Gongtian Shen**, China Special Equipment Inspection and Research Institute, Beijing 100013, China. Contact e-mail: zhangzh@buaa.edu.cn.
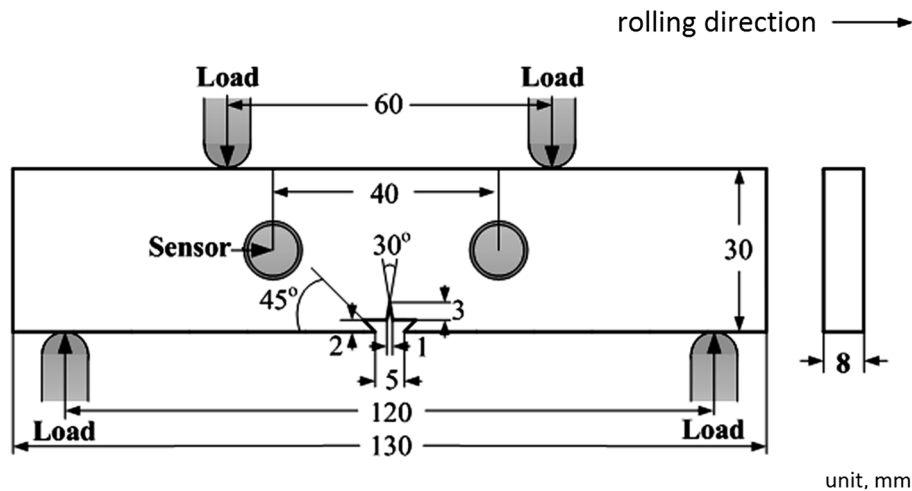
Fig. 1 Dimensions of four-point bending fatigue specimen showing AE sensor position

2. Material and Experiments

2.1 Material and Specimens

Hot-rolled commercial pure titanium (CP-Ti), Grade 2 (0.028Fe, 0.009C, 0.002H, 0.009N, 0.11O, all in wt.%) was used for the experiments. The four-point bending specimens were machined parallel to the rolling direction, and the dimensions are shown in Fig. 1. To obtain a variation of grain size, the specimens were sealed in quartz tubes under vacuum and subjected to one of the following heat treatments: (a) annealed at 923 K for 2 h and air-cooled to room temperature and (b) annealed at 1073 K for 10 h and furnace cooled. The mechanical properties of the three conditions from tensile tests are given in Table 1. The initial microstructures of all investigated specimens exhibited nearly equiaxed grains in a single α-phase without twin.

2.2 Fatigue Test and Microscopic Observation

Fatigue crack propagation tests were carried out on a servo-hydraulic testing machine (Model: 8801, Instron Ltd., Britain) at room temperature (300 K). The tests were performed under sinusoidal cyclic loading at a frequency of 10 Hz, with a load ratio of 0.1 and a peak load of 8 kN. The loading positions are shown in Fig. 1. A standard crack tip opening displacement (CTOD) gage with an accuracy of 0.01 mm was used to measure the crack length. The stress intensity factor range ΔK was calculated from the crack length simultaneously. After the crack growing to an a/W of 0.6-0.7 (a is the crack length, W is the width of the specimen), or the amount of AE signals presenting a fast exponential increase, which AE activity implies a beginning of crack unstable growth, the tests were terminated. Then, the specimens were sectioned parallel to the major plane of the sheet to examine metallographically the fracture-face profiles, and the fatigue-fracture surfaces were observed by scanning electron microscopy (SEM, Model: JSM-5800, JEOL, Japan). Transmission electron microscopy (TEM) and electron backscattered diffraction (EBSD) were performed for microstructure observation. The samples prepared for TEM and EBSD were both by the following procedure. The samples were mechanically polished and further thinned in a TenuPol-5 twin-jet electropolisher with an electrolyte consisting of 5%

perchloric acid, 35% butoxy-ethanol, and 60% methanol solution at −20 °C and 9 V (Ref 15). TEM was carried out using a JEOL JEM-2100 operating at 200 kV. EBSD was conducted by a JEOL SEM-6500F and analyzed with Channel 5 software from HKL Corporation for texture and twin analysis.

2.3 Acoustic Emission Monitoring

AE monitoring was performed using a DiSP-4/PCI AE system (Physical Acoustic Corporation, USA). Two piezoelectric sensors with a bandpass from 100 to 900 kHz were used to pick up the AE signals. The sensors were attached to the specimen by an adhesive tape using vaseline as the coupling agent and their positions are shown in Fig. 1. A band pass filter, with a range of 100-1200 kHz, was used in the preamplifier. An amplitude threshold of 40 dB was set. Determined by a dummy specimen without a notch, an AE energy threshold of 1 mV μs and an average frequency threshold of 35 kHz were set to eliminate the mechanical noise, which were the same thresholds with the previous study in our lab (Ref 16). A linear AE source location was used to make sure that the obtained signals were generated from the crack area.

## 3. Results and Analysis

3.1 Fatigue Crack Propagation

The development of a fatigue crack is commonly divided into three stages as follows: (1) crack initiation, (2) crack stable propagation, and (3) crack unstable growth. For Stage 2, the crack propagation obeys the Paris law

$$da/dN = M(\Delta K)^n, \, or \, \log(da/dN) = \log M + n \cdot \log(\Delta K),$$
$$(Eq \ 1)$$

where a is the crack length, N is the fatigue cycle number, ΔK is the stress intensity factor range, and M and n are assumed to be constants for a given material. Experimental crack propagation rate da/dN and the Paris constants M and n according to Eq 1 for specimens with different grain sizes are presented in Fig. 2 and Table 2. During Stage 1, da/dN increased with the grain size for the same ΔK. However,

Table 1   Mechanical properties of CP-Ti with three different grain sizes

	Average grain size, D, μm	Yield stress, MPa	Ultimate tensile stress, MPa	Elongation, %	Area reduction, %
As received	26	329.4	395.9	25.7	50.8
Heat treatment					
(a)	45	295.1	369.1	24.5	43.8
(b)	93	274.7	332.5	23.9	42.5
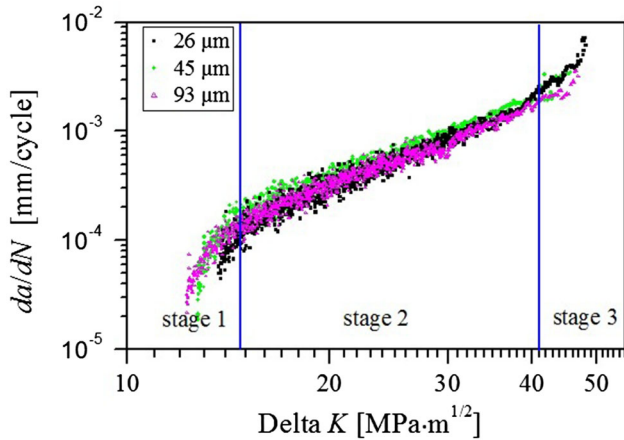
Fig. 2 Relationships between da/dN and ΔK for specimens with three different grain sizes

da/dNs for all the three conditions were almost overlapped during Stage 2 (Fig. 2). The Paris exponent n is around 2-4, which is in the same range for other metal materials (Ref 9, 16). It can be seen that n decreased slightly as the grain size increased (Table 2).

3.2 Microstructural Characterization

3.2.1 Microstructure.   Texture determinations by EBSD showed that the specimens with different average grain sizes have similar initial textures. After fatigue tests, the textures adjacent to the crack edge during Stage 2 were changed, but only subtly. The pole figures of the $D = 45$ μm sample are shown in Fig. 3. It is seen that the texture evolution is characterized by the shift of the two strong maxima from the former TD to RD in the {0 0 0 1} pole figure. The value of the maximum increased from 4.44 before to 6.69 after the fatigue test.

During Stage 2, deformation twins were found with two kinds of microscopic morphology in the side of the fracture. The EBSD scanning images for the $D = 45$ μm sample are shown in Fig. 4 to reveal the twin morphology, which are located on the right side of the crack, about 90 μm from the main crack edge. One type of twin with a lenticular shape (Fig. 4a) was observed in all specimens with three different grain sizes; it was dispersedly located near the crack, and the quantity decreased with the distance to the crack. Moreover, the number of lenticular twins increased with grain size. The other type of twin (twin paling) with a straight and narrow shape (Fig. 4b) was found in a local area along the edge of the crack; the density and intersection of the twin paling increased with grain size. The lenticular twin type was found to be the {10 $\bar{1}$2} twin, and the twin paling type is found to be the {11 $\bar{2}$2} or {10 $\bar{1}$2} twins. These results imply that the twin activity varied with the crystal grain size during the fatigue crack stable

Table 2   Experimental constants M and n for specimens with three different grain sizes

D, μm	log M	n
26	−7.21	3.09
45	−7.01	2.97
93	−6.57	2.71

propagation. However, only recently, the presence of twins has been suggested as an interface control mechanism in coarsely grained metal, and is considered a relevant microstructural feature that influences fracture (Ref 17).

3.2.2 Fracture Surface.   Typical scanning electron micrographs of the fracture surfaces of the specimens with three different grain sizes are shown in Fig. 5 for different periods of Stage 2. The direction of the crack propagation was from the left to the right. The micrographs indicate that the crack propagation was transgranular, and that the fracture was featured by a mix of cleavage and ductile dimple fractures. In early Stage 2 with $\Delta K < 20$ MPa m$^{1/2}$ (see Fig. 5a, c, and e), the morphology and the volume fraction of the intrinsic features on the surfaces were not found to vary with the grain size. In late Stage 2 with $\Delta K > 30$ MPa m$^{1/2}$ (see Fig. 5b, d, and f), the fracture surfaces all showed fatigue slip striations. Marked by the white arrows, it can be seen in Fig. 5 (d)-(f) that some local small fracture planes were twin boundaries.

3.3 AE During Fatigue Testing

3.3.1 AE Activity.   The AE activities are illustrated in Fig. 6 and 7. Figure 6 shows a plot of the normalized cumulative AE counts C_{cum} versus the normalized loading cycles N. According to the first and the last inflection point of the slope, the AE activities can also be divided into three stages. Such division into three AE stages during fatigue has also been observed in many other materials (Ref 9, 16, 18). In such materials, C_{cum} first grew rapidly over a short period (Stage 1). This was followed by slower growth rates with lesser and weaker AE activity for a rather long period (Stage 2). Finally, C_{cum} increased markedly again (Stage 3). In the present work, C_{cum} also increased rapidly during Stages 1 and 3. However, C_{cum} did not grow steadily during Stage 2.

In order to study the AE feature of the fatigue crack stable propagation, several attempts have been made to relate AE counts rate to material fatigue crack behavior (Ref 16, 18, 19). During Stage 2, an equation similar to Eq 1 has been proposed to relate AE counts rate dC/dN to ΔK (Ref 9, 16):

$$dC/dN = P(\Delta K)^q, \ or \ \log(dC/dN) = \log P + q \log(\Delta K),$$
$$(\text{Eq 2})$$

where C is the number of AE counts, and P and q are assumed to be constants for a given material. Figure 7(a)-(c)
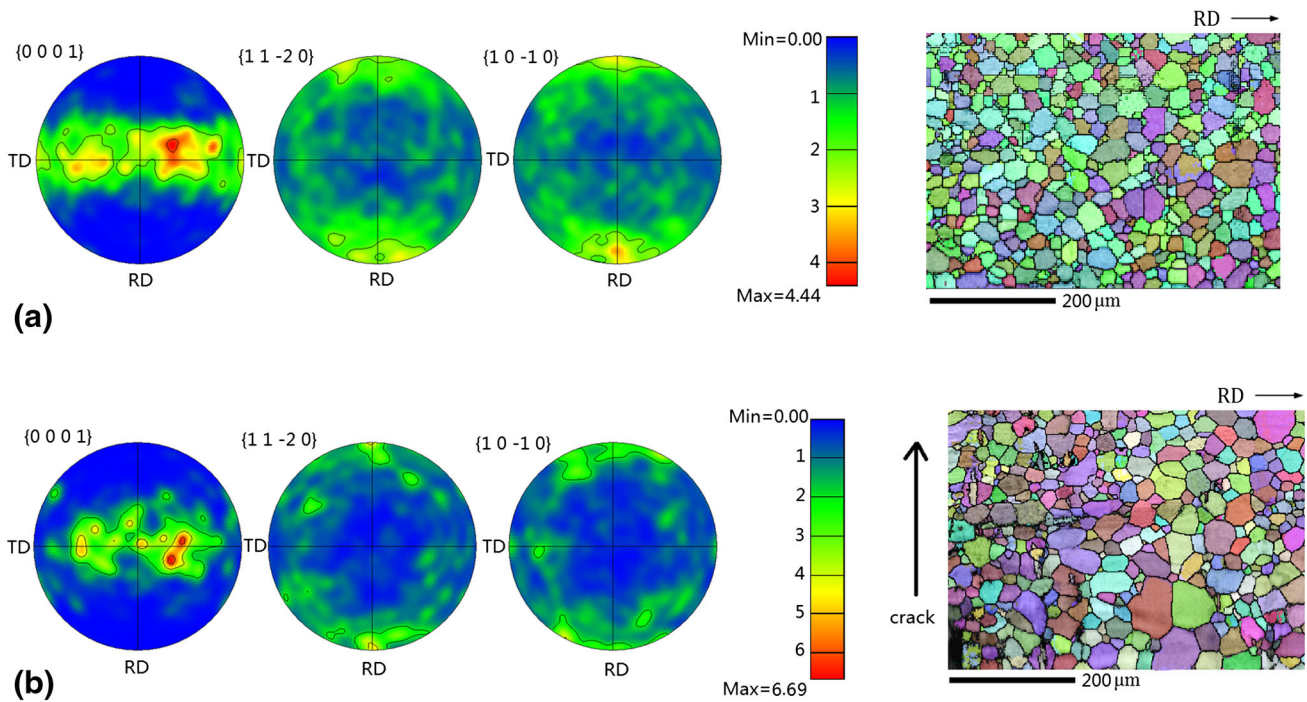
Fig. 3 EBSD pole figures for the $D = 45$ μm sample, (a) before and (b) after fatigue fracture

shows the correlograms of dC/dN versus ΔK for specimens with different grain sizes on double logarithmic axes. Comparing Fig. 6-7 with Fig. 2, it is noted that the AE signals in the AE Stage 2 are ascribed mainly to crack stable propagation. It is also seen that higher dC/dN is observed in specimens with larger D. During the AE Stage 2, dC/dN increasing with ΔK was no longer in a perfect linear relationship. There appeared to be some obvious local fluctuations. There were more fluctuations in the specimens with larger grain sizes than in the specimens with smaller grains. However, without consideration of the fluctuations, dC/dN versus ΔK can still be generally seen as a line. The experimental P and q, based on Eq 2, are listed in Table 3. For the investigated material, which is a mostly pure metal of a single phase, no trace of periodic crack rapid growth or any visible transition area was observed over the whole fatigue fracture. The crack propagation in Stage 2 was relatively stable and steady. This indicates that different AE mechanisms occurred during the linear and the fluctuating parts.

3.3.2 AE Source Mechanisms During Stage 2. More attention was paid to the local areas associated with the fluctuations. By relating the specific ΔK at the local fluctuation to the corresponding N and thus the crack length a, the microstructure referred to the local area can be approximately located in the metallograph of a side-view of the fatigue surface and in the scanning electron micrograph of the fatigue surface. The optical metallographs of the specimen with $D = 45$ μm presented in Fig. 8 illustrate this. It should be noted that the related metallographs were not easy to obtain, because the twin paling was only at the edge of the crack. Due to the edge effect of the crack, electrolytic polishing, which would cause the electrolysis process to act especially on the crack, was difficult to apply. Another difficulty was that the crack width was wide
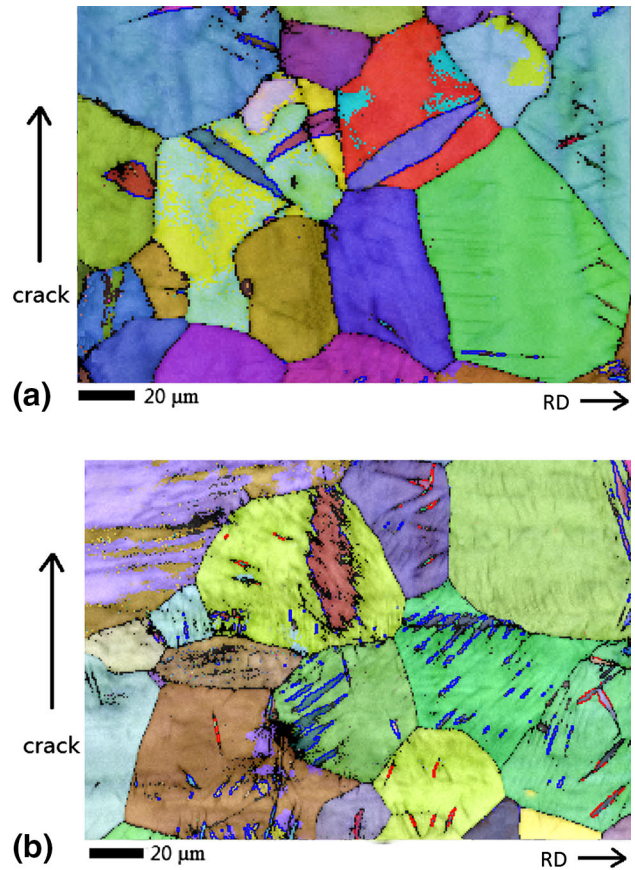

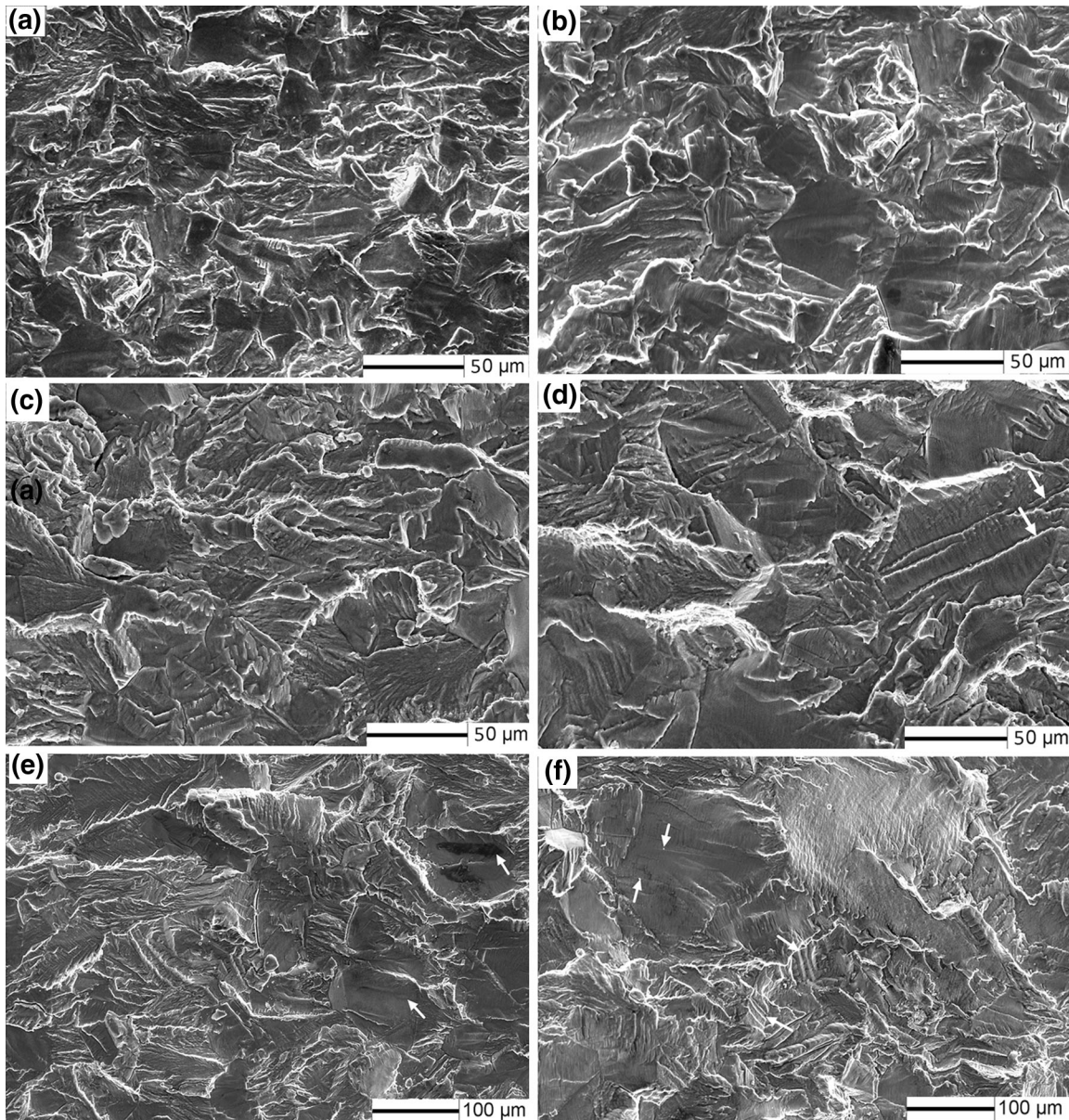**Fig. 4** EBSD observation for the $D = 45$ μm sample showing (a) lenticular-shaped twins and (b) twin palings

Fig. 5 Scanning electron micrographs of fracture surfaces for specimens with grain size of $D = 26$ μm (a, b), $D = 45$ μm (c, d), and $D = 93$ μm (e, f) during early Stage 2 with $\Delta K < 20$ MPa m$^{1/2}$ (a, c, e) and late Stage 2 with $\Delta K > 30$ MPa m$^{1/2}$ (b, d, f)
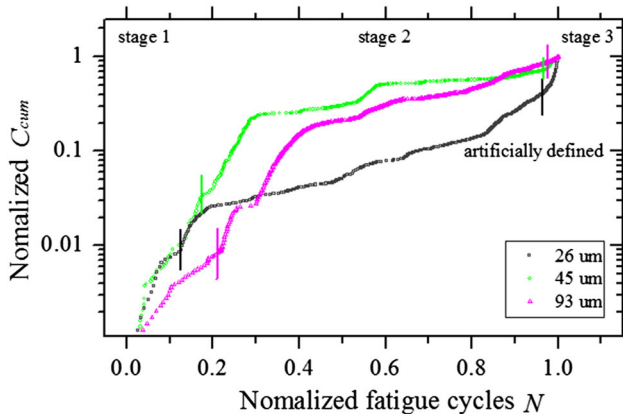

Fig. 6 Normalized AE counts C_{cum} versus fatigue cycles N

near the notch. Care must be taken to avoid more etching solution absorbing around the wider crack, and overflowing while observing. Moreover, the existing twin paling exacerbated the retention of the etching solution. Based on Fig. 8, it can be seen that these local areas had more severe crack deflection features or furcation accompanied with some twin palings converged.

Figure 9 shows the corresponding fatigue surfaces at different areas in the $D = 45$ μm specimen during Stage 2; the direction of the crack propagation is indicated by an arrow. Figure 9(a) focuses on the microstructure away from the fluctuation area, and Fig. 9(b) focuses on the local fluctuation. The circular region shows typical morphology of a lenticular twin, and the rectangular region shows a twin paling. The fracture-traversing twin paling formed a series of very small steps. This indicates that when the plastic deformation of the crack tip accumulated to a certain degree, the slip and lenticular
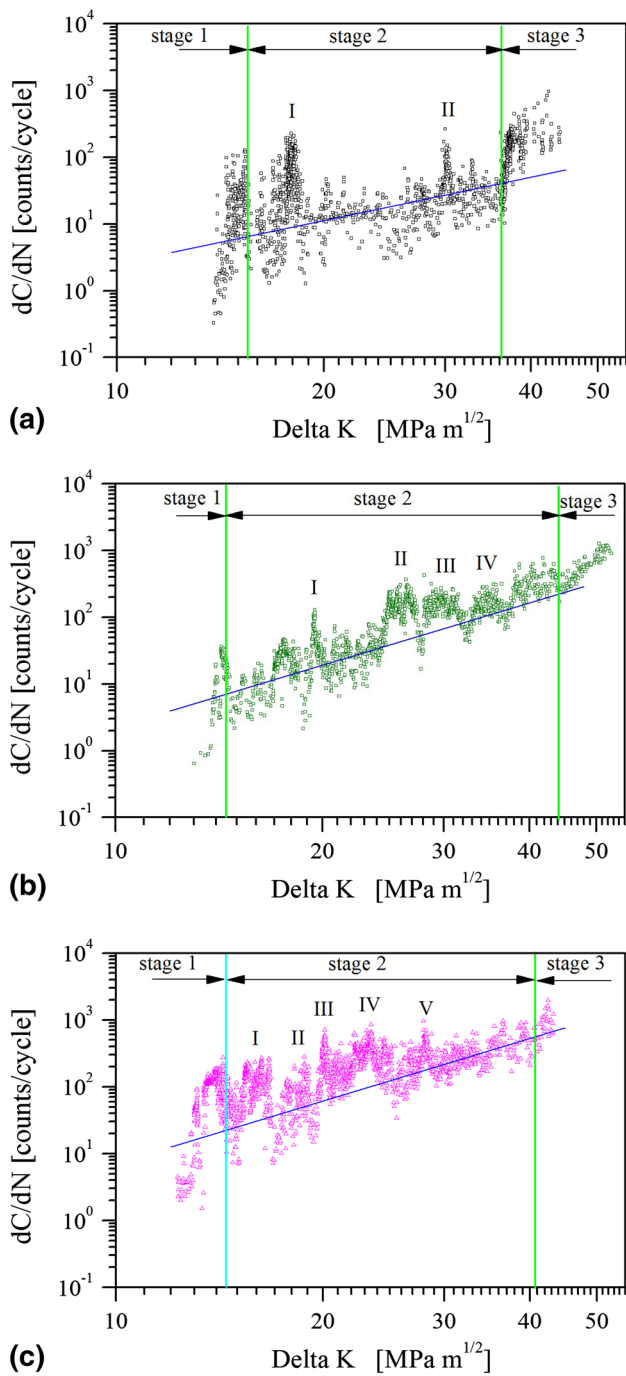
Fig. 7 Relationships between dC/dN and ΔK

Table 3 Experimental constants P and q for specimens with three different grain sizes

D, μm	log P	q
26	−1.76	2.16
45	−2.74	3.08
93	−2.24	3.10

twin were insufficient for relieving the plastic strain. Thus, twin paling with dense twins appeared. The interface between the parent grain and the twin paling was beneficial to the crack propagation, which formed several small steps/facets in the fracture surface. Figure 10 shows the typical twins near the crack edge of the $D = 45$ μm specimen during Stage 2 by TEM; a higher density of dislocation existed around the twin paling than around the lenticular twin. It can be seen that twin boundaries act as barriers to dislocation motion and can cause dislocation line coalescence or crack branching, which would result in the propagation of the fracture along the interface or crack deflection. Therefore, based on the above, the AE signals contributing to the linear part of Fig. 7 should be related to the crack extension itself and to the lenticular twins; on the other hand, the AE signals related to the local fluctuations should be derived from the twin palings. Of course, crack extension itself has several micromechanisms, such as plastic zone extension and crack closure, which are also the sources of AE. Such AE mechanisms always coincide with crack development, and thus cannot be responsible for the sharp ups and downs of the dC/dN fluctuations in Fig. 7. Differentiation between the AE from the plastic zone extension and from the crack closure is very difficult, and is not discussed in this paper.

4. Discussion

4.1 Grain Size Effect on Fatigue Crack Stable Propagation

The behavior of fatigue crack stable propagation obeys the Paris law. In theory, the Paris law is an empirical equation rather than a constitutive one. The two Paris constants M and n depend on the material properties and test environment. Recently, some researchers have tried to explain the physical nature of the Paris equation. By means of dislocation dynamic theory, thermal activation, and velocity process theory, the two constants were determined theoretically and explained by Liu et al. (Ref 20). Based on the microscopic structural parameters of the material and the testing conditions, they described the Paris law as follows:

$$da/dN = \frac{A_0}{f^\lambda} \exp\left(-\frac{\lambda U}{kT}\right)(\Delta K)^{\left(1+\frac{\alpha}{kT}\right)\lambda}, \qquad (Eq\ 3)$$

$$M = \frac{A_0}{f^\lambda} \exp\left(-\frac{\lambda U}{kT}\right), \qquad (Eq\ 4)$$

$$n = \lambda + \frac{\lambda\alpha}{kT}. \qquad (Eq\ 5)$$

In Eq 3 to 5, f is the loading frequency, k is the Boltzmann constant, T is the absolute temperature, and U and α are the material constants. The latter two are derived according to the activation energy of the material by $H = U - \alpha ln(\Delta K)$, where H is the activation energy required for a dislocation segment to overcome the Peierls hills based on the Seeger's double kink model (Ref 21). Additionally from Eq 3 to 5, $A_0 = b\gamma(m)\left(\frac{A}{4bG\epsilon^{1/2}}\right)^\lambda$, $\lambda = \frac{m+1}{m+2}$, A is a material constant related to the specimen's geometry, b is Burgers
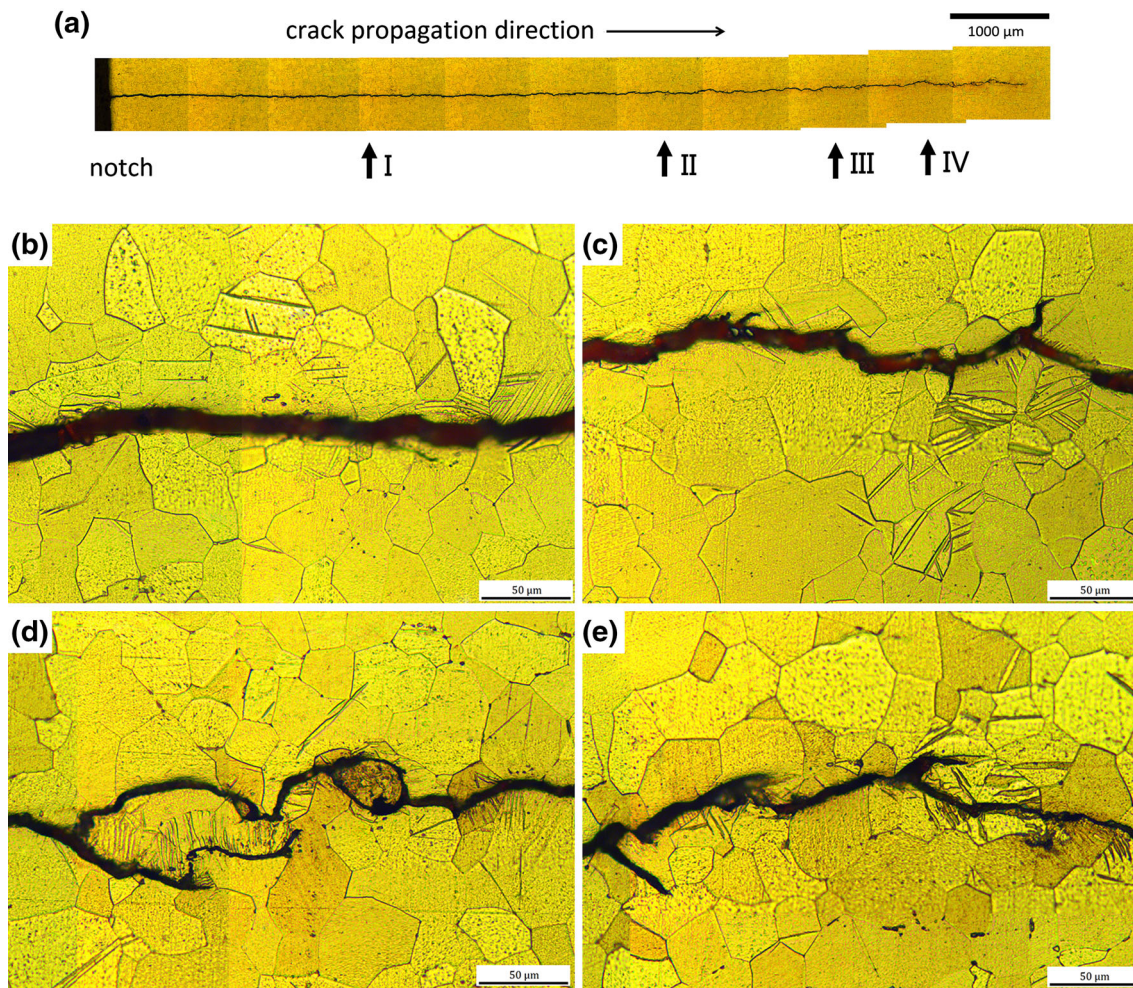
Fig. 8 Optical metallographs around the AE dC/dN local fluctuations for the $D = 45$ µm specimen, (a) the whole crack, (b) area I, (c) area II, (d) area III, and (e) area IV

vector, G is shear modulus, and ε is the displacement under the average stress (and is constant under a given condition). The variable m is the exponent in the dislocation velocity formula given by

$$\upsilon = \upsilon_0 (\tau_a / \tau_o)^m, \qquad (\text{Eq } 6)$$

where τ_a is the applied shear stress, υ_0 is a constant velocity, and τ_o is the stress required to produce υ_0 (Ref 21). Finally, $\gamma(m)$ is a function of m, and for a metal material, $\gamma(m) = 1.396 \text{ m}^{-1.45}$ (Ref 22). Thus, for a given initial state of a material and a particular test condition, M is a constant.

Substituting the definition of λ into Eq 5, the following is obtained:

$$n = \frac{m+1}{m+2}\left(1 + \frac{\alpha}{kT}\right) = B(T)\frac{m+1}{m+2}, \qquad (\text{Eq } 7)$$

where $B(T)$ is a constant under a given test temperature. Thus, n is closely related to m

$$n = B\frac{m+1}{m+2} = B\left(1 - \frac{1}{m+2}\right). \qquad (\text{Eq } 8)$$

Therefore, Eq 4 and 8 reveal the physical nature of the Paris law. It should be noted that the above deduction was based only on dislocation activity. In the present work, although mechanical twin appeared along the crack, $da/dN-\Delta K$ still obeyed the Paris law. The main two reasons for this are as follows: (1) the crack length a is a measured value at the macro-level, and it cannot represent the actual damage mechanism of the crack and (2) the crack stable propagation is accomplished dominantly by dislocation motion. Increasing rain size would cause the velocity of dislocation motion υ to decease (Ref 23). Based on Eq 6, decreased υ results in the decrease of m and the increase of λ. Thus, M increases and n decreases. This is consistent with the results in Fig. 2 and Table 2. Because m is an exponent in Eq 6, its increase with grain size should be limited, and then the changes in M and
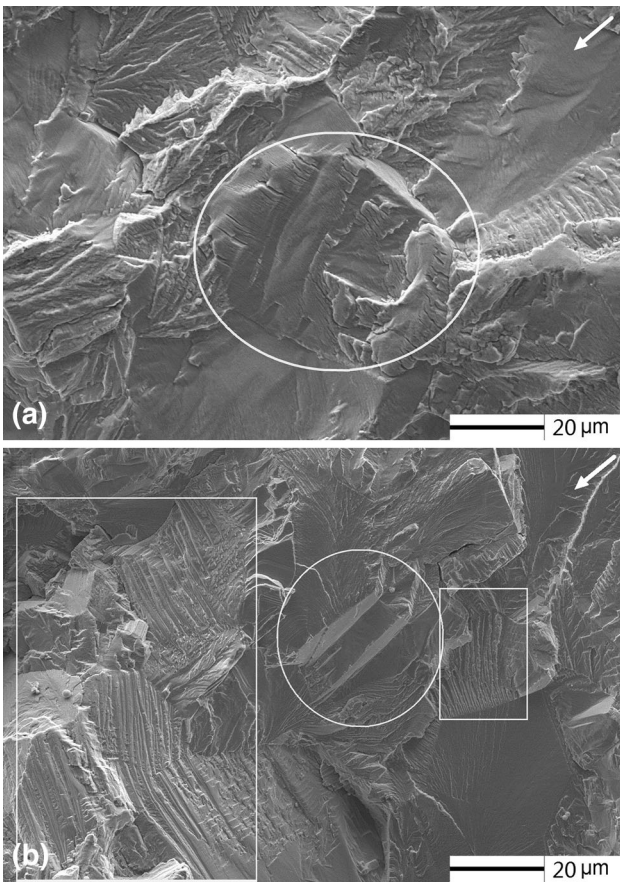
Fig. 9 Fatigue surfaces of the $D = 45$ μm specimen that included (a) lenticular twin and (b) twin paling

Fig. 10 TEM observation near the crack edge of the $D = 45$ μm specimen (a) lenticular twin and (b) twin paling

n are slight. Furthermore, increased M and decreased n have the opposite effect on da/dN. Therefore, da/dN would change weakly with grain size. For macroscopic crack propagating in metal with conventional grain sizes, a da/dN that is independent of grain size has been reported for many materials (Ref 4, 8, 24, 25).

4.2 Grain Size Effect on AE During Stage 2

The dC/dN is a value measured by AE that reflects the activity of an AE source. Dislocation motion has long been confirmed to be a conspicuous AE source in metal under stress. Therefore, in CP-Ti with dislocation acting as the dominant fatigue mechanism, the relationships of $dC/dN-\Delta K$ and $da/dN-\Delta K$ should follow the same rule as the Paris law. Bigger grain means larger area of the crack tip plastic zone, which results in higher dC/dN per unit of ΔK. In *hcp* metals, twin has been observed as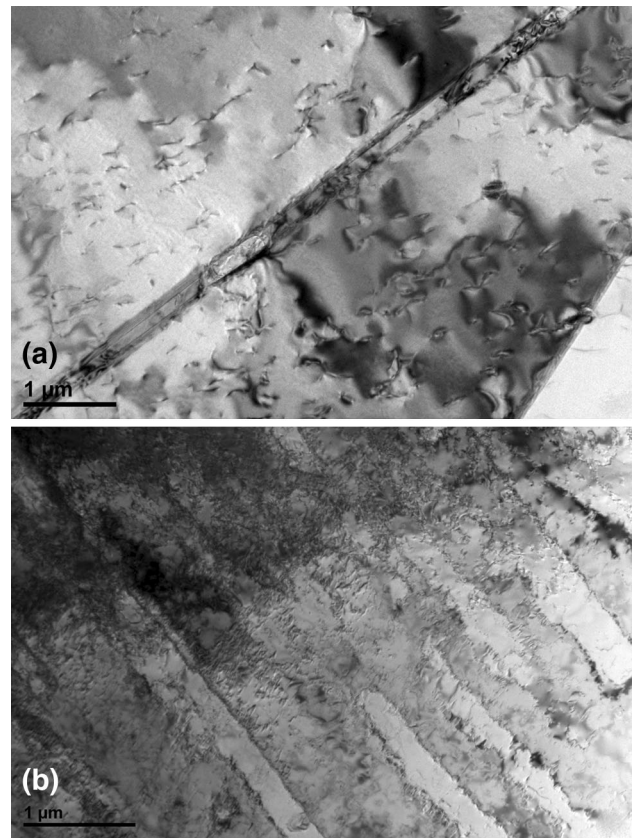 another notable AE source (Ref 26). In the present work, a small number of lenticular twins occurred consistently with the crack growth, while a few twin palings appeared intermittently. Therefore, during Stage 2, because dislocation motion is the principal damage mechanism with twin palings assisting periodically, the AE $dC/dN-\Delta K$ not only presented a general linear rise that obeys the Paris law, but also showed some local fluctuations stemming from the activity of twin paling. Twinning in titanium has a greater tendency to occur in samples with larger average grain size (Ref 27). In this work, the amount of the lenticular twin, and the position and quantity of the twin paling increased with the grain size. A twin can be modeled as a pile-up of dislocations that have moved rapidly within a parent grain. This suggests that twin is associated with higher energy and higher frequency of the corresponding AE signal (Ref 26). Therefore, the local fluctuations of $dC/dN-\Delta K$ caused by twin paling showed much higher dC/dN and higher frequency. The typical waveform and power spectral density (PSD) are illustrated in Fig. 11.
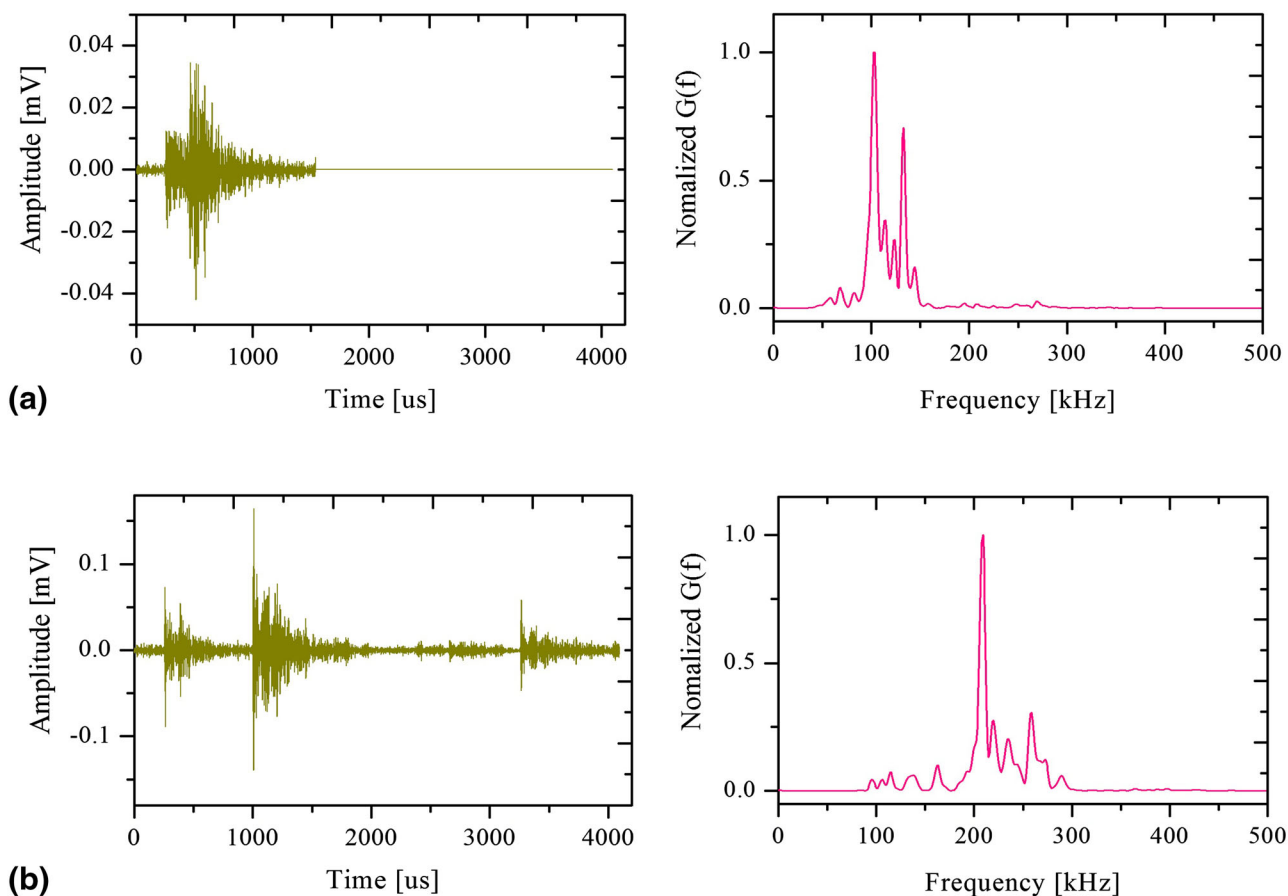
Fig. 11 Typical AE waveform and PSD during Stage 2, (a) without $dC/dN-\Delta K$ fluctuation and (b) with $dC/dN-\Delta K$ fluctuation

5. Conclusion

(1) During the stage of crack stable propagation, the curves of $da/dN-\Delta K$ in commercial pure titanium with three grain sizes all obeyed the Paris law. The crack propagation rate was almost independent of the grain size.

(2) For the fatigue crack development, the AE activities ($dC/dN-\Delta K$) were divided into three distinct stages, which can be related to the three stages of the curve of $da/dN-\Delta K$. During the fatigue crack stable propagation, the AE counts rate dC/dN increased with the grain size increase.

(3) The plastic deformation ahead of the crack tip was accomplished mainly by dislocation motion and subserviently by deformation twin. There were two morphologies of twins, lenticular twin with a twin type of $\{10\ \bar{1}2\}$, and twin paling with a twin type of $\{11\ \bar{2}2\}$ or $\{10\ \bar{1}2\}$.

(4) The AE activity was sensitive to the changes in the microstructure, which were due to the fatigue damage accumulation. The plot of $dC/dN-\Delta K$ has a linear trend that was the result of the dislocation motion and the occurrence of lenticular twin. Local fluctuation areas of the $dC/dN-\Delta K$ plot were the result of the twin paling.

References

1. Y. Ono, T. Yuri, H. Sumiyoshi, S. Matsuoka, and T. Ogata, Effect of Grain Size on High-Cycle Fatigue Properties in Alpha-Type Titanium Alloy at Cryogenic Temperatures, *Cryogenics*, 2003, **43**(8), p 483–489

2. E. Kerscher, Influence of Microstructure and Micro Notches on the Fatigue Limit, *Proc. Eng.*, 2014, **74**, p 210–217

3. X. Demulsant and J. Mendez, Microstructural Effects on Small Fatigue Crack Initiation and Growth in Ti-6A1-4V Alloys, *Fatigue Fract. Eng. Mater. Struct.*, 1995, **18**(12), p 1483–1497

4. K. Tokaji, T. Ogawa, and K. Ohya, The Effect of Grain Size on Small Fatigue Crack Growth in Pure Titanium, *Int. J. Fatigue*, 1994, **16**(8), p 571–578

5. K. Tokaji, J.C. Bian, T. Ogawa, and M. Nakajima, The Microstructure Dependence of Fatigue Behaviour in Ti15Mo5Zr3Al Alloy, *Mater. Sci. Eng. A*, 1996, **213**(1–2), p 86–92

6. G.R. Yoder, L.A. Cooley, and T.W. Crooker, Quantitative Analysis of Microstructural Effects on Fatigue Crack Growth in Widmanstätten Ti-6A1-4V and Ti-8Al-1Mo-1V, *Eng. Fract. Mech.*, 1979, **11**(4), p 805–816

7. J.L. Robinson and C.J. Beevers, The Effects of Load Ratio, Interstitial Content, and Grain Size on Low-Stress Fatigue-Crack Propagation in α-Titanium, *J. Metal Sci.*, 1973, **7**, p 153–159

8. B. Oberwinkler, Modeling the Fatigue Crack Growth Behavior of Ti-6Al-4V by Considering Grain Size and Stress Ratio, *Mater. Sci. Eng. A*, 2011, **528**(18), p 5983–5992

9. T.M. Roberts and M. Talebzadeh, Acoustic Emission Monitoring of Fatigue Crack Propagation, *J. Constr. Steel Res.*, 2003, **59**(6), p 695–712

10. S. Mostafavi, M. Fotouhi, A. Motasemi, M. Ahmadi, and C.T. Sindi, Acoustic Emission Methodology to Evaluate the Fracture Toughness in Heat Treated AISI, D2 Tool Steel, *J. Mater. Eng. Perform.*, 2012, **21**(10), p 2106–2116

11. M. Huang, L. Jiang, P.K. Liaw, C.R. Brooks, R. Seeley, and D.L. Klarstrom, Using Acoustic Emission in Fatigue and Fracture Materials Research, *JOM-e*, 1998, **50**(11), p 1–14

12. D.H. Kohn, P. Ducheyne, and J. Awerbuch, Sources of Acoustic Emission during Fatigue of Ti-6Al-4V: Effect of Microstructure, *J. Mater. Sci.*, 1992, **27**(6), p 1633–1641

13. S. Mashino, Y. Mashimo, T. Horiya, M. Shiwa, and T. Kishi, Analysis of Microfracture Mechanism of Titanium Alloy by Acoustic Emission Technique, *Mater. Sci. Eng. A*, 1996, **213**(1–2), p 66–70

14. D.H. Kohn, P. Ducheyne, and J. Awerbuch, Acoustic Emission during Fatigue of Ti-6Al-4V: Incipient Fatigue Crack Detection Limits and Generalized Data Analysis Methodology, *J. Mater. Sci.*, 1992, **27**(12), p 3133–3142

15. D.R. Chichili, K.T. Ramesh, and K.J. Hemker, The High-Strain-Rate Response of Alpha-Titanium: Experiments, Deformation Mechanisms and Modeling, *Acta Mater.*, 1998, **46**(3), p 1025–1043

16. Z.Y. Han, H.Y. Luo, Y.B. Zhang, and J.W. Cao, Effects of Microstructure on Fatigue Crack Propagation and Acoustic Emission Behaviors in a Micro-alloyed Steel, *Mater. Sci. Eng. A*, 2013, **559**(1), p 534–542

17. P. Cavaliere, Fatigue Properties and Crack Behavior of Ultra-Fine and Nanocrystalline Pure Metals, *Int. J. Fatigue*, 2009, **31**(10), p 1476–1489

18. M. Talebzadeh and T.M. Roberts, Correlation of Crack Propagation and Acoustic Emission Rates, *Key Eng. Mater.*, 2001, **204–205**, p 341–350

19. M.N. Bassim, Detection of Fatigue Crack Propagation with Acoustic Emission, *NDT&E Int.*, 1992, **25**(6), p 287–289

20. L.M. Liu, M.L. Duan, C.T. Liu, and H.J. Zhao, On the Physical Nature of the Paris Law, *Acta Mech. Sin.*, 2003, **35**(2), p 172–175

21. H.L. Prekel and H. Conrad, Dislocation Velocity Measurements and Thermally Activated Motion in Molybdenum, *Acta Metall.*, 1967, **15**(5), p 955–958

22. T. Yokobori, A.T. Yokobori, Jr., and A. Kamei, Dislocation Dynamics Theory for Fatigue Crack Growth, *Int. J. Fract.*, 1975, **11**(5), p 781–788

23. C.R. Heiple and S.H. Carpenter, Acoustic Emission Produced by Deformation of Metalsand Alloys—A Review: Part I, *J. Acoust. Emiss.*, 1987, **6**, p 177–204

24. R. Wright and A.S. Argon, Fatigue Crack Growth in Si-Fe, *Metall. Trans.*, 1970, **1**(11), p 3065–3074

25. G. Birkbeck, A.E. Inckle, and G.W.J. Waldron, Aspects of Stage II, Fatigue Crack Propagation in Low-Carbon Steel, *J. Mater. Sci.*, 1971, **6**(4), p 319–323

26. A. Vinogradov, D. Orlov, A. Danyuk, and Y. Estrin, Effect of Grain Size on the Mechanisms of Plastic Deformation in Wrought Mg-Zn-Zr Alloy Revealed by Acoustic Emission Measurements, *Acta Mater.*, 2013, **61**(6), p 2044–2056

27. M.A. Meyers, O. Vöhringer, and V.A. Lubarda, The Onset of Twinning in Metals: A Constitutive Description, *Acta Mater.*, 2001, **49**(19), p 4025–4039